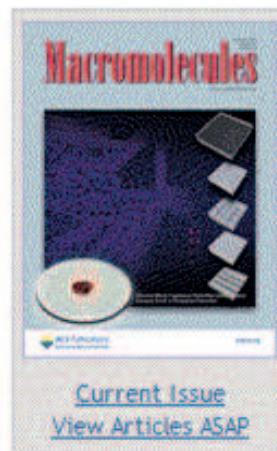


Short-Range Order in Polyethylene Melts: Identification and Characterization

José A. Martins* and Nuno M. Micaelo



2012 Impact Factor **5.521**

Editor: [Timothy P. Lodge](#)

- » [Editors & EAB](#)
- » [About the Journal](#)
- » [Recommend This Journal](#)
- » [Author Index](#)

ACS Divisions

- » [Polymer Chemistry](#)
- » [Polymeric Materials: Science & Engineering](#)

ADVERTISEMENT

Free 
Access
to 2013
Sample Issues

 ACS Publications

[Articles ASAP](#) [Current Issue](#) [Most Read](#)





 [RSS feed](#)

Articles ASAP (As Soon As Publishable)

ASAP articles are edited and published online ahead of print.

Now showing 1-5

[View All](#)

☐  View Abstracts  Add to ACS ChemWorx  Download Citations 


Synthesis of Optically Active Poly(*m*-phenyleneethynylene-aryleneethynylene)s Bearing Hydroxy Groups and Examination of the Higher Order Structures

Hiromitsu Sogawa, Masashi Shiotsuki, Takehiro Hirao, Takeharu Haino, and Fumio Sanda

Articles ASAP (As Soon As Publishable)

[Abstract](#) | [Supporting Info](#)

 [ACS ActiveView PDF](#)
Hi-Res Print Annotate Reference QuickView

 [PDF \[4609K\]](#)

 [PDF w/ Links \[511K\]](#)

 [Full Text HTML](#)

Materials SCENE 

materials
SCENE

Countdown To The 2013
Chemistry Nobel Prize
Events
October 07, 2013

Grinding Out Reactions
Boosts Catalytic Rate
October 07, 2013

Rock On With Carbon
Nanotubes
October 07, 2013



Access your research
from anywhere.

Add articles to ACS
ChemWorx to access your
research from anywhere.

Browse By Issue

Select Decade 

Select Volume 

Select Issue 

[List of Issues](#)

[GO](#)

Short-Range Order in Polyethylene Melts: Identification and Characterization

José A. Martins^{*,†,‡} and Nuno M. Micaelo[§]

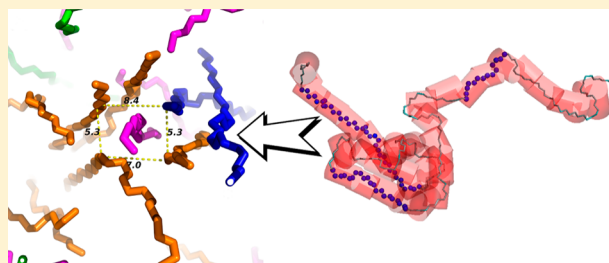
[†]Departamento de Engenharia de Polímeros, Universidade do Minho, Campus de Azurém 4800-058 Guimarães, Portugal

[‡]CICECO, Universidade de Aveiro, 3810-193 Aveiro, Portugal

[§]Departamento de Química, Centro de Química, Universidade do Minho, Campus de Gualtar 4710-057 Braga, Portugal

S Supporting Information

ABSTRACT: Experimental results by Fisher et al. [*Faraday Discuss. Chem. Soc.* **1979**, *68*, 26] showed the existence of local orientational correlations of segments of the *n*-alkane molecules in the liquid state. Since the estimated correlation volume is below 10^3 \AA^3 , molecular dynamics simulations appear to be a suitable method for their identification and characterization. We used molecular dynamics to fully characterize short-range order in polyethylene melts. The characterization started by identifying sequences of aligned segments in chains, each one having at least one Kuhn monomer in length. Afterward, a search was made for interactions of a tagged aligned chain segment with others fulfilling the same condition, laying within a limiting separation distance (18 Å) and making a limiting orientation angle (40°). When, at least, four interactions are counted, a short-range ordered region is defined. Chain placement in these regions has similarities to that of the unit cell at the solid phase, although with different separation distances and angle. Overall, short-range order resembles a dynamic uniaxial nematic phase, the local order parameter increasing with the chain length in agreement with experimental results. Segments at the ordered regions persist over time, for times longer than the Rouse relaxation time of the chain. Those in random conformational sequences between the ordered regions have a mass distribution in agreement with the Flory distribution, with a number-average value comparable to experimental results for the molecular mass between entanglements.



1. INTRODUCTION

To quote Flory: “The arrangement of long-chain molecules in condensed phases is a subject that has evoked intense controversy. Two divergent viewpoints have been propounded with respect to the liquid or amorphous state, including glasses. The issues at stake are of strategic importance; molecular interpretation of the properties of polymers obviously requires an understanding of morphology at the molecular level”.¹ By this time, arguments supporting the existence of order in polymer melts were contested by “the formidable body of evidence supporting the prevalence of randomness in molten and amorphous states”.¹ Among them, is a self-consistent field argument presented by de Gennes² which basically states that the outward force acting on the segments of a test chain located close to its center of gravity, where their concentration is higher, is compensated by another force resulting from segments of other chains present in the same region, due to their lower concentration. The overall force acting on the test chain is thus zero, and hence the chain remains ideal.

The current picture of melt morphology emerged from this evidence. It is considered that chains in polymer melts are unperturbed, behaving as ideal. Energetic interactions involving segments of the same, or different, chains are inexistent, and changes in chains’ free energy result only from entropic variations originated by changes in chain conformations. Chains

of ideal chain models consist of immaterial links, each one joined to two nearest neighbors, having no interactions with solvent molecules or with other links of the same, or another chain. In concentrated solutions or polymer melts, it is considered that entanglements between chains act as topological restrictions to chain motion. Entanglement effects on the flow of polymer melts are described by tube model, reptation movement and several additional mechanisms.^{3,4}

At the present, it is generally accepted that polymer melts are nearly ideal. Deviations from ideality have been ascribed to long-range intramolecular correlations,^{5,6} and to the existence of short-range order. Some recent results indicating “solid-like” behavior (or short-range order) in melts^{7,8} have generated controversy.^{9,10} The argument is that the experiments in their basis were performed in the limit of the instruments’ working conditions, casting doubts on the results validity.

Apparently uncontroversial experimental results demonstrating the existence of short-range order can be classified in three types. The first are those of phenomenological nature, such as the work of Zondervan et al.¹¹ that can only be understood if short-range order is considered to exist in the liquid phase. In

Received: May 14, 2013

Revised: August 1, 2013

Published: September 24, 2013

the second type we include the experiments by Fisher et al.¹² that quantified short-range order with a correlation volume—below (10 Å)³—and also those by the group of Spiess that quantified this order with an order parameter ($S = 0.2$),¹³ and assigned to the heterogeneities present in the melt a dynamic length scale (≈ 30 Å).¹⁴ Finally, other works provided finer details on short-range order by quantifying the separation distance for intermolecular interactions. In this class we include the wide-angle X-ray diffraction experiments of Londono et al.¹⁵ that demonstrate for polyethylene melts the existence of intermolecular correlations at 4 Å. A similar result was also obtained by Mitchell et al.¹⁶ that assigned the breadth of diffuse interchain peaks in scattering patterns from melts to the limited spatial correlation between chain segments, concluding further that correlated segments consisted of three to four skeletal bonds in the trans conformation.

The first known work on the evaluation of short-range order by molecular dynamics simulations in *n*-alkane chains dates back to 1988. Rigby and Roe modeled sequences of 10 and 20 CH₂ groups in ensembles of 500 or 2000 united atoms.¹⁷ Force-fields used are similar to those of more recent works.¹⁸ They evaluated the intermolecular radial distribution function and the orientational correlation function at different temperatures for different sets of CH₂ units, from 1 up to 10 (for the chain with 20 segments). It was found that the height of the peaks in the radial distribution function decreases by increasing the number of segments considered in the chains and temperature. On the other hand, by decreasing temperature the peak positions shift to slightly shorter distances and the peaks shapes sharpen. Results for the orientational correlation function showed a similar behavior, and demonstrated that in the simulated melts there exists a significant degree of short-range order. The authors concluded that, on a very local scale, a short-subchain is surrounded by a bundle of about seven parallel subchains. Furthermore, the finding that the degree of order increases by decreasing temperature led the authors to evaluate a temperature for the “possible” isotropic–nematic phase transition.

The buildup of nematic order was also found by Weber et al.¹⁹ in Monte Carlo simulations of dense polymer melts. The Hamiltonian used in these simulations favors stretched bond angles and short bonds, naturally yielding therefore a Gaussian coil at high temperatures and a rigid rod at very low temperatures. Short-range order in polymer liquids was accessed also by Abrams and Kremer²⁰ with molecular dynamics simulations of bead–spring models. They analyzed the ratio of bond length to excluded volume bead diameter, l_0/d_0 , on the equilibrium structure of bulk melts composed of freely joined bead–spring polymer chains. It was found that the characteristic disorder existing when $l_0/d_0 < 1$ disappears for $l_0/d_0 > 1$. In this last case, if bonds are long enough, significant intermolecular correlations exist, and the polymer fluid can display high short-range order. It was concluded then that the manner in which excluded volume is distributed along a chain of simple spheres determines the intermolecular structure in dense liquids of these chains.

Here we identify and characterize short-range order in polymer melts. We started by simulating a melt of density as similar as possible to available experimental results. Chains of different length were simulated with the united atom representation, and their characteristic ratio was evaluated at different temperatures. Since models used in the description of the flow behavior consider the Kuhn monomer as the basic

repeating chain unit, the Kuhn statistical segment length, l_k , and the Kuhn monomer diameter, d_k , were evaluated at each temperature. The only assumption made in the definition of short-range order is that aligned chain segments (ACS) may be defined by confining all chain segments to a tube of diameter lower than d_k . After this definition, a search is made for interactions of a tagged ACS with other ACS belonging to the same chain or to other chains, located at a reasonable separation distance, and making with the tagged ACS a reasonable orientation angle. As explained in section 3.2 below, the distance and angle are determined by correlations in the radial distribution function and by the order parameter of the nematic phase, respectively. Results of this search are presented below.

We start with a detailed explanation of the molecular dynamics simulation procedure. Results obtained are compared with those available in the literature for similar systems. The aligned chain segments’ definition, and the labeling procedure used in the identification of short-range order are presented with detail. The short-range order is fully characterized, and the lifetime of segments belonging to these regions is accessed. Additional evaluation details are included in the Appendix and in the Supporting Information.

2. SIMULATION DETAILS

2.1. Building of the Polymer Systems. The molecular dynamics simulations were performed in a cluster composed by 62 nodes with dual socket dual core AMD Opteron Processor 280. All modeling and simulation procedures of polyethylene (PE) chains followed closely that of Paul et al.,^{18,21} also followed by Gee et al.²² These chains were modeled using a united atom representation that reduces the polymer to its skeleton, the backbone carbon atoms. Polymer melt systems with different chain lengths and number of chains were assembled into a cubic box having around 160³ Å³. Strictly monodisperse assembled systems were as follows: C₅₀H₁₀₂, 2800 chains; C₁₀₀H₂₀₂, 1400 chains; C₂₅₀H₅₀₂, 560 chains, and C₅₀₀H₁₀₀₂, 280 chains. The molecular mass of chains in these systems covers a broad range, from 702 g/mol up to 7002 g/mol. Literature values for the PE entanglement molecular mass range from ≈ 828 g/mol up to ≈ 1850 g/mol.^{23,24} After a detailed testing of different methods for the M_e evaluation, 1200 g/mol was considered a good estimate for M_e .²³ The critical molecular mass is between $2M_e \leq M_c \leq 3M_e$.²⁴ Each one of the above systems was simulated at six different temperatures: 353, 373, 393, 415, 500, and 600 K.

A single chain of C₅₀₀H₁₀₀₂ was initially created in a fully extended (all-trans) configuration and subjected further to 10 ps of unrestrained molecular dynamics simulation (see below for details). The system of 280 chains of C500 was then built by replicating the initial chain 279 times in a cubic box using packmol.²⁵ Each chain was randomly placed in the box by translation and rotation of their united atoms. The assembled system was energy minimized using the conjugate gradient method and stopped if no further minimization was possible (within the machine single precision limit) or if it reached a maximum of 20000 steps. Afterward, the system was equilibrated at 415 K. Total energy and density reached equilibration within 150 ns of simulation, which is also the time for the diffusion of the chain across a distance comparable to $\langle R_g^2 \rangle$ at 415 K. At 600 K, this time reduces to ~ 100 ns. As described by Brown et al.,^{26,27} the time for melt equilibration could have been established also by evaluating the time

Table 1. Force Field Energy Functions and Parameters—See Table I in Paul et al.¹⁸

bonded interactions	energy functions	parameter values
bond lengths	constrained	$l_{C-C} = 1.53 \text{ \AA}$
bond angles	$V_a(\theta_{ijk}) = \frac{1}{2} k_{ijk}^a (\theta_{ijk} - \theta_{ijk}^0)^2$	$k_{ijk}^a = 502.08 \text{ kJ mol}^{-1}$; $\theta_{ijk}^0 = 110$
torsions	$V_F(\phi_{ijkl}) = \frac{1}{2} \left\{ \begin{aligned} &C_1[1 + \cos(\phi)] + \\ &C_2[1 - \cos(2\phi)] + \\ &C_3[1 + \cos(3\phi)] \end{aligned} \right\}$	$C_1 = 6.694 \text{ kJ mol}^{-1}$, $C_2 = -3.627 \text{ kJ mol}^{-1}$, $C_3 = 13.556 \text{ kJ mol}^{-1}$
nonbonded interactions	$V_{LJ}(r_{ij}) = 4\epsilon_{ij} \left[\left(\frac{\sigma_{ij}}{r_{ij}} \right)^{12} - \left(\frac{\sigma_{ij}}{r_{ij}} \right)^6 \right]$	$\epsilon_{ij} = 0.469 \text{ kJ mol}^{-1}$, $\sigma_{ij} = 4.5 \text{ \AA}$, $V_{LJ}(r_{ij}) = V_{LJ}(9 \text{ \AA})$ for $r_{ij} > 9 \text{ \AA}$

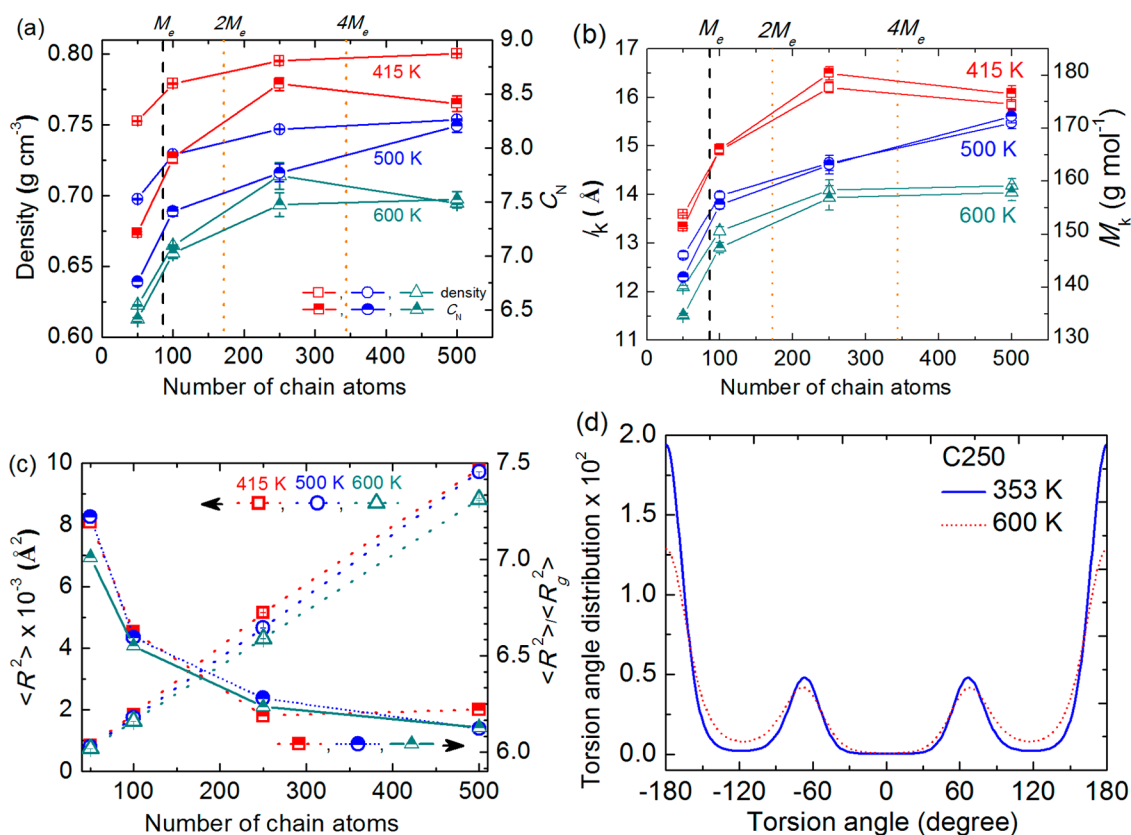


Figure 1. Chain length variation of the mean values for the physical parameters characterizing the simulated systems at the indicated temperatures. Error bars of the mean are indicated. (a) Density and chain characteristic ratio. (b) Length and molecular mass of one Kuhn monomer. (c) Mean-square end-to-end distance, $\langle R^2 \rangle \propto n$, and ratio $\langle R^2 \rangle / \langle R_g^2 \rangle$. (d) Torsion angle distribution for two different temperatures; *trans* conformation corresponds to the torsion angle of $\pm 180^\circ$.

variation of the mean percentage of *trans* dihedral angles, or of the mean squared radius of gyration. Since these two last properties usually stabilize around a well-defined mean value in a much shorter time scale, and because the objective of this work was also studying dynamic properties of well equilibrated melts, the time scale for melt equilibration was set to $g_1(\tau_1) = \langle R_g^2 \rangle$.^{27,28}

The C250, C100 and C50 systems were built from the equilibrated system C500 at 415 K by splitting these chains two, five and ten times, respectively, and terminating each smaller chain with a CH₃ molecule at both ends. All these new systems, including those created at other temperatures, reached energy and density equilibration after 20 ns of simulation. Both potential energy and density attained rapid convergence within the first nanoseconds. Molecular dynamics simulations were

then performed over all equilibrated systems at different temperatures for an additional 100 ns.

2.2. Force Fields and Simulations. Table 1 contains the parameters and force field energy functions used in the simulations. All bonds in the polymer chain were constrained to the equilibrium lengths used by the force field with LINKS algorithm.²⁹ Dihedral torsion potential was modeled in terms of a Fourier function. The proper dihedral angles definition used is that of Gromacs,³⁰ which follows the IUPAC convention, where ϕ is the angle between the *ijk* and *jkl* planes, with zero corresponding to the *cis* configuration. The equation is the same as that in Table 1 of ref 18 which uses the convention $\phi_{trans} = 0$. Nonbonded interactions were truncated at 9 Å, and the neighbor list was updated every five integration steps. Equations of motion were integrated with the leapfrog

algorithm with an integration step of 2 fs. All systems were simulated in the isothermal–isobaric ensemble at the pressure of 1 atm. The temperature was coupled to a heat bath using the Nose–Hoover thermostat³¹ and pressure with the Parrinello–Rahman method.³² Temperature and coupling constants used were 0.2 and 0.5 ps, respectively. Molecular dynamics simulations were performed with the GROMACS 4.5.3 program.³⁰

Figure 1 displays the variation with the chain length of physical parameters characterizing the simulated systems. Temperature variation of the experimental density is represented in Figure 2. Polynomial equations describing this

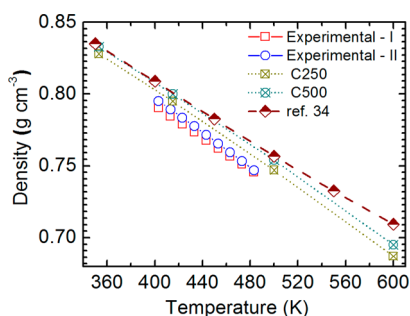


Figure 2. Temperature variation of the experimental density for linear polyethylene in the temperature window between 350 and 600 K according to two different equations of ref 33. Values of Figure 1a for C250 and C500 are also indicated, together with results from ref 34 obtained by molecular dynamics simulations—half-filled lozenges.

variation in a temperature window between 403 and 480 K were obtained from ref 33. Differences between the simulated and experimental results agree, both in temperature and molecular weight dependencies, with those of other molecular dynamics simulation results.³⁴ The chain characteristic ratio C_N was evaluated for each system from $C_N = 6\langle R_g^2 \rangle / nl$, where $\langle \cdot \rangle$ is a time and ensemble average, R_g the radius of gyration, n the number of chain atoms, and l the C–C bond length.

Both density and chain characteristic ratio (C_N) increase with molecular mass and, similarly to other polymer properties, such as melting temperature and glass transition temperature,³⁵ stabilize at a nearly constant value for chains of mass value above the critical molecular mass (Figure 1a). As a result, variation of the Kuhn monomer length and mass with the chain length follows a similar trend (Figure 1b). The Kuhn monomer length and mass were evaluated from requirements imposed to the “real”, unperturbed, chain and to the equivalent chain: $\langle R^2 \rangle_0 = \langle R^2 \rangle_{eq}$ and $R_{0,max} = R_{max,eq}$.³⁶ From these requirements one obtains $l_k = C_N l / \sin(\theta/2)$ and $M_k = C_N M_{UA} / \sin^2(\theta/2)$, where M_{UA} is the mass of the united atom and θ the valence angle. For chains of infinite mass C_N saturates at $C_N = C_\infty$.

The linear variation of the mean-square end-to-end distance with the chain length is represented in Figure 1c, together with the ratio $\langle R^2 \rangle / \langle R_g^2 \rangle$. These results demonstrate that all simulated entangled chains (C250 and C500), for all temperatures, behave nearly as predicted for Gaussian coils—ratio $\langle R^2 \rangle / \langle R_g^2 \rangle \cong 6$. Deviations from ideal behavior are lower than 5%. The mean values were taken from frames recorded each 0.1 ns during the last 100 ns of the simulation after equilibration (total of 1000 frames). For unentangled chains (C50 and C100) deviations from ideality may be as high as 21.6%.

The characteristic ratio for chains of infinite mass, $C_\infty = \langle R^2 \rangle / nl^2$ was evaluated for all temperatures from the slope of $\langle R^2 \rangle$ versus n in Figure 1c, yielding the results of Table 2, that

Table 2. Characteristic Ratio Values at Different Melt Temperatures Used in the Definition of Kuhn Monomer Length and Number of United Atoms Existing within One Kuhn Monomer and in the Packing Length Evaluation

T (K)	C_∞
353	8.812 ± 0.035
373	8.993 ± 0.070
393	8.979 ± 0.108
415	8.560 ± 0.193
500	8.366 ± 0.067
600	7.514 ± 0.037

agree with results obtained with the procedure described in ref 34. These results were used in the definitions of the minimum number of segments (C–C bonds) existing in one ordered chain segment at each temperature, as well as in the definitions of Kuhn monomers at the different parts of the chain (chain ends, ordered regions and in random conformational sequences between the ordered regions). Specifically, for these evaluations we considered $M_k = C_\infty M_{UA} / \sin^2(\theta/2)$ and the number of C–C bonds in one Kuhn monomer was evaluated by taking the integer part of M_k / M_{UA} . The effect of this procedure is that we are imposing longer Kuhn monomers in the systems of shorter chains (C50 and C100), ≈ 2 Å more, the other systems remaining unaffected by this choice.

The torsion angle distribution was also evaluated for the lowest and highest temperature used in the simulations. The results depicted in Figure 1d are mean values for an ensemble and time average (time interval of 100 ps), and they agree with those of Alexiadis et al.³⁷ for similar melt temperatures. Integration of the curves between -180° to -120° and between 120° and 180° yields the fraction of trans conformations. The percentage of trans conformers is 61.26% at 600 K and 67.39% at 353 K.

3. RESULTS

3.1. Identification of Aligned Chain Segments (ACS).

Once ensured the agreement between these simulation results and those of other authors, illustrated in Figures 1 and 2 and in others below, the identification of short-range order was performed. To locate short-range order we started by devising a procedure for identifying sequences of ordered segments. It was considered that each chain may be described by a statistical equivalent chain as a sequence of n_k Kuhn monomers, each one of length l_k ; segments in this statistical chain are also confined by a tube of diameter d_k —the Kuhn monomer diameter.

To demonstrate this confinement, the chain is broken in Kuhn monomers. Further, the distance, d , between each atom within one Kuhn monomer (line 2 in Figure 3a) and the line joining the first and last atoms of the Kuhn monomer (line 1) is evaluated. The result of this mapping for the ensemble of 560 chains and C250 at three different temperatures (353, 415, and 600 K) is depicted in Figure 3b. It shows the normalized distribution for the separation distance of all chain atoms to a vector defining one Kuhn monomer, as illustrated in Figure 3a, running over all atoms, in Kuhn monomer steps. The normalization factor is the number of Kuhn monomers in the ensemble. Contrary to expected, the distribution of d values is

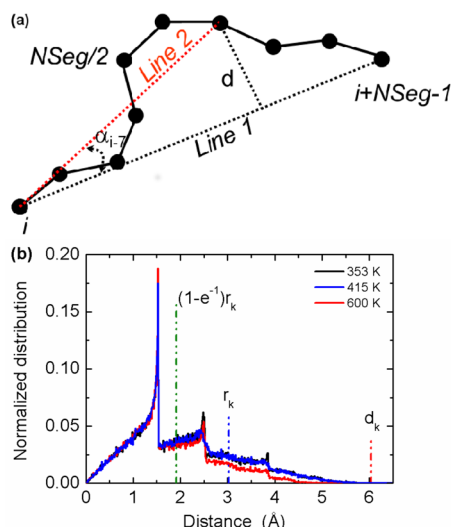


Figure 3. (a) Procedure used in the definition of aligned chain segments. d is the distance between a united atom within one Kuhn monomer (line 2) and the line joining the first and last atoms of one Kuhn monomer (line 1). (b) Distribution of d values evaluated for all chain atoms within one Kuhn monomer, with the exception of the first and last one, normalized by all Kuhn monomers in the ensemble. Values indicated are for the system of 580 chains of C250. The maximum d value is the Kuhn monomer diameter, d_k . Ordered sequences are defined confining atoms to a thinner tube, eq 2.

not uniform, or peaked around a mean value. It is rather peaked at around 1.5 Å; this value, however, has nothing to do with the C–C bond length. Note that the distance d in Figure 3b is $d = \sin(\alpha_{ij})/|r_{ij}|$. The Kuhn monomer diameter, d_k , is the maximum value of d . This diameter may be evaluated also from the packing length definition³⁸ using the self-similarity property of Gaussian chain segments assumption

$$p = \frac{V_{\text{chain}}}{\langle R^2 \rangle_0} = \frac{M_{\text{chain}}}{\langle R^2 \rangle_0 \rho N_{\text{Av}}} = \frac{n_k M_k}{\langle R^2 \rangle_0 \rho N_{\text{Av}}} = \frac{V_k}{l_k^2} = \frac{\pi d_k^2}{4 l_k} \quad (1)$$

where p is the packing length, $\langle R^2 \rangle_0$ the unperturbed mean-square end-to-end distance and ρ the melt density. Each Kuhn monomer may then be viewed as a cylinder of diameter d_k , length l_k , and volume $V_k = M_k/\rho N_{\text{Av}} = \pi d_k^2 l_k/4$. Table S1 at the Supporting Information shows values evaluated for the packing length and Kuhn monomer diameter at two representative temperatures. As shown, changes in d_k become significant only for shorter chains and higher melt temperatures. Values for the packing length agree with experimental results,³⁸ and with others obtained by molecular dynamics simulations of similar systems.³⁹

Data in Figure 3b suggest a cutoff distance (thinner tube diameter) for defining aligned chain segments. Virtually, any value of d between the first peak value (1.5 Å) and the Kuhn monomer diameter, d_k , may be used for that definition. After several testing, the thinner tube diameter was set at $(1 - e^{-1})d_k/2$. It is ensured with this selection that for all systems and temperatures the thinner tube diameter is always set at a distance just above the first peak. From eq 1, since $d_k = (4pl_k\pi^{-1})^{1/2}$, the critical distance separating the atoms within one Kuhn monomer to line 1 was then set to $d_{\text{crit}} = (1 - e^{-1})d_k/2$,

$$d_{\text{crit}} = (4pl_k\pi^{-1})^{1/2}(1 - e^{-1})/2 \quad (2)$$

Aligned chain segments (ACS) defined with eq 2 are represented in Figure 4, which shows tube sections of diameter

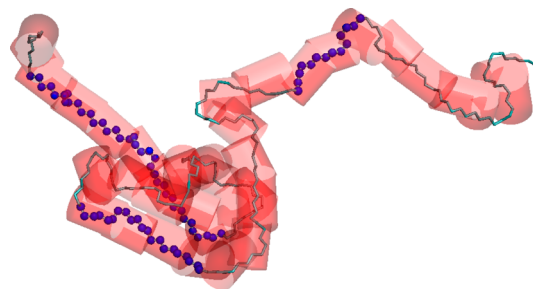


Figure 4. Selected chain of C250 with three aligned chain segments (ACS), identified as balls, and defined with eq 2. Each ACS is identified with a label as Label (chain number, initial atom, final atom), where the Label is an integer value giving the number of ACS existing in a specific chain.

d_{crit} running in steps of $n_k^0/2$, where $n_k^0 = M_k/M_{\text{UA}}$ is the number of chain segments within one Kuhn monomer. This running step was considered to allow for some gauche conformations within one aligned chain segment. A sample of the code used in this evaluation is provided in the Supporting Information. Besides the confinement of chain segments to a thinner tube, an additional restraint was used to define aligned chain segments. It was further required that the number of segments in these sections should be at least equal to those existing in one Kuhn monomer. Aligned chain segments in Figure 4 are represented by balls and they are mainly sequences of atoms in trans conformations.

3.2. Identification of Short-Range Order. Identification and labeling of ordered chain segments and, at a later stage, of short-range ordered regions was inspired by the Hoshem–Kopelman algorithm.⁴⁰ Once identified an ACS sequence, it is labeled as Label (chain number, initial atom, final atom). For a particular chain, the Label value indicates the existing number of ordered segments, being zero for chains without ordered sequences. Following the labeling, a search is made for interactions of a tagged ordered sequence with other ordered sequences belonging to the same chain, or to other chains.

Three additional constraints were considered in this search: (i) the separation distance between chains segments should be within a distance where correlations are recorded in experiments and simulations for the radial distribution function (18 Å); (ii) the angle between interacting chain segments must be constrained to the lowest value of the order parameter for a nematic phase^{41,42} $S = \langle P_2(\mathbf{n} \cdot \mathbf{n}_i) \rangle = 0.4$, where \mathbf{n} is the director and \mathbf{n}_i the unit vector of the i th molecule, and (iii) a chain segment should interact with the other four, at least, to define a short-range ordered region (the PE unit cell contains five chain segments).

Only a reduced number of chain segments fulfill these conditions. They were additionally labeled, and selected as being part of the short-range ordered regions. Figure 5a maps the ordered chain segments after the last labeling, where segments having one to four, or more, interactions are drawn with different colors. During this labeling, segments of some chains, at the boundary of an ordered region, having therefore fewer interactions, were excluded from it for not fulfilling the third condition—chain marked with * in Figure 5b. A final labeling process was then implemented for aggregating

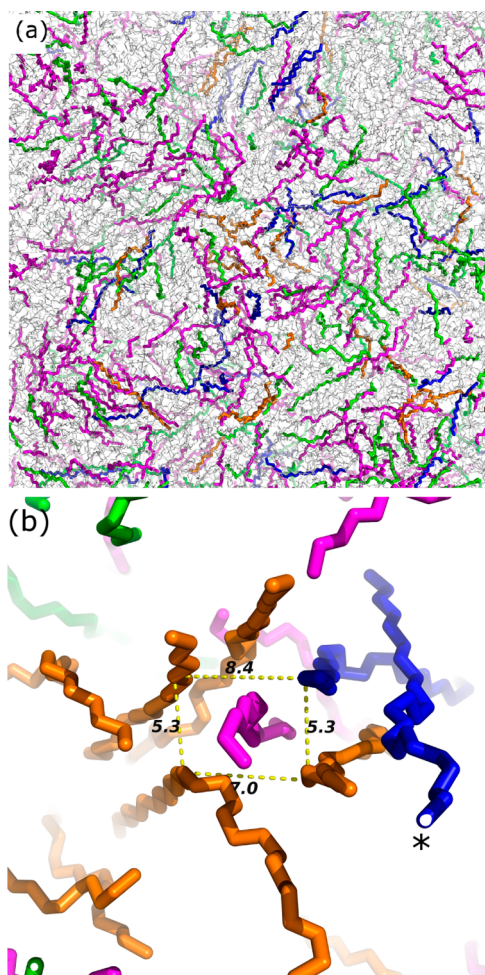


Figure 5. (a) Ordered chain segments after the second labeling process (sticks). Segments in random conformational sequences excluded from the thinner tube in Figure 4 are indicated by gray. Different colors distinguish segments having different number of interactions. Magenta is for a binary interaction (two segments only), green, blue and orange are for interactions involving three, four, five, or more than five, ordered segments, respectively. (b) Magnification of part a (center) and showing a close view of a local ordered region. The asterisk labels a segment at the boundary of the ordered region excluded from it during the second labeling process.

previously excluded chain segments and defining the short-range ordered region.

Figure 5b shows how a short-range ordered region looks like. Similarly to short-range order in liquids,⁴³ the spatial arrangement of segments in the first coordination shell is dominated by repulsive intermolecular forces, and resembles that existing in the orthorhombic PE unit cell, at the solid phase. Below we analyze the ordered regions dimensions, structure, stability and orientational dynamics.

3.3. Structural Characterization of Short-Range Order.

The number of both aligned chain segments (ACS) and local ordered regions (LOR) per chain increases with the melt temperature and chain length (Figure 6a). Note that the number of ACS per chain increases with temperature and chain length, and their distribution is peaked around a mean value. On the contrary, the number of LOR per chain, while increasing also with temperature and chain length, shows a distinct variation. For C500, from a total of 280 chains, ordered regions have been identified only in $\approx 36\%$ of them.

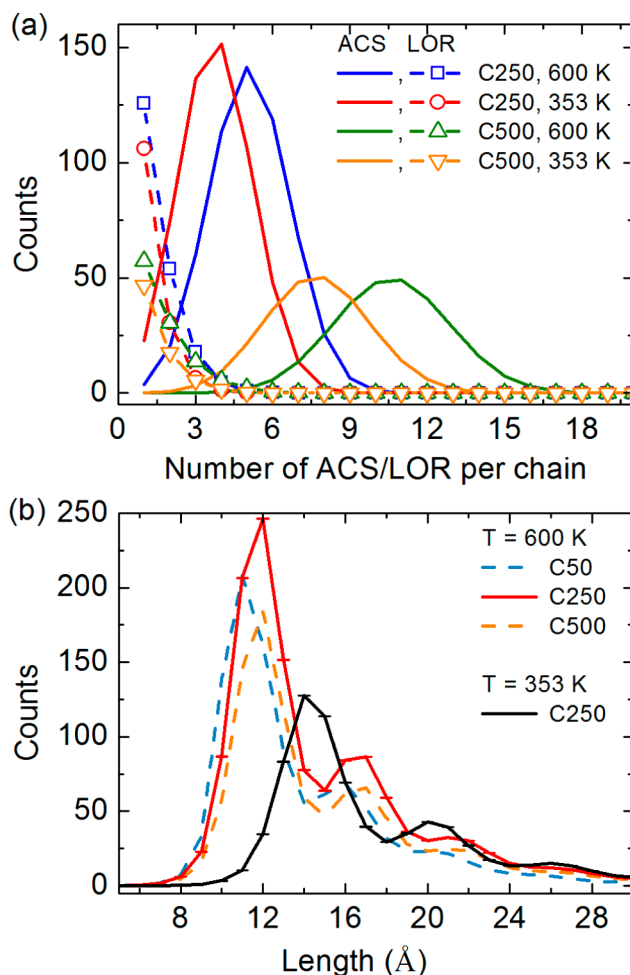


Figure 6. (a) Number of ordered segments per chain after the first (ACS – full lines) and last (LOR- dashed lines and symbols) labeling processes; UA = number of united atoms. Mean results of 4500 data files over an equilibration time of 100 ns. Error bars have the line thickness size. (b) Ordered regions length variation for systems C50, C250, and C500 at the lowest (353 K) and highest (600 K) simulation temperature.

Ordered regions are shorter at higher temperature (Figure 6b), which is explained by the increase in the population of gauche conformational states, yielding a lower volume fraction of chain segments in the LOR. As for the LOR thickness distribution, it increases with the lowering of temperature, encompassing a range from one to more than two Kuhn monomers, agreeing with previous estimates⁴⁴ based on the analysis of experimental data, ≈ 18 Å. The peaks in the thickness distribution are ascribed to the algorithm used in the identification of aligned chain segments. As explained in section 3.1, the search for aligned chain segments within the thinner tube is made in steps of $n_k^0/2$.

A typical volume fraction of the initially defined aligned chain segments (ACS) is $\approx 35\%$ at 353 K and $\approx 25\%$ at 600 K, while the volume fraction of chain segments in the LOR is between 4.5% and 2.5%, respectively (evaluations made for a limiting angle between the interacting chain segments of 40° , corresponding to $P_2 = 0.4$). On average, only around 10% of the initially defined ACS participates at each time in the LOR. Since the average number of both ACS and LOR is almost constant along time and, as demonstrated below, the number of LOR identified at time zero decreases slowly with time, we

conclude that segments in the LORs are rejuvenated along time; they may migrate to a random conformational sequence, to a chain end, and/or simply being replaced by other neighboring ACS.

LORs are almost spherical in shape at high temperature and become more elongated as temperature decreases, acquiring the shape of a prolate ellipsoid. Table 3 contains the eigenvalues of

Table 3. Eigenvalues of the Radius of Gyration Tensor and of the Order Tensor for the Local Ordered Regions^a

	C250		C500	
	353 K	600 K	353 K	600 K
R_{g11}	20.02	13.49	22.01	14.63
R_{g22}	14.64	10.71	14.45	11.01
R_{g33}	10.98	8.56	9.88	8.46
Q_{11}	0.24	0.18	0.31	0.22
Q_{22}	−0.02	−0.01	−0.04	0.02
Q_{33}	−0.22	−0.17	−0.27	0.20

^aFor all evaluations, the standard error of the mean is a factor 10^{-3} of the mean value. Units of R_g eigenvalues are in Å.

the LORs' radius of gyration tensor (evaluation made according to the description in Appendix I) as well as those of the order tensor (see Appendix II). For C500, and $T = 353$ K, the local order tensor eigenvalues are $Q_{11} = 0.31$, $Q_{22} = -0.04$, $Q_{33} =$

−0.27, consistent with a local “dynamic” uniaxial nematic phase.⁴⁵ Similar dynamic local order parameter values ($Q_{11} = 0.34$), were experimentally evaluated by fast field cycling NMR studies on the dispersion of the ^1H spin–lattice relaxation time of linear 1,4-polybutadienes - see ref 46 and Figure S1 of Supporting Information.

Oriental correlations (see Appendix III) of chain segments in the melt and at the ordered regions are presented in Figure 7a. The figure shows the second order Legendre polynomial $\langle P_2(\alpha) \rangle_r = \langle 3(\mathbf{u}_i \cdot \mathbf{u}_j)^2 - 1 \rangle / 2$, where \mathbf{u}_i and \mathbf{u}_j are unit vectors of chain segments connecting the UA participating in the LOR (including those of the same chain), and the ensemble average is taken over all LOR identified in one time frame, and over all frames recorded after equilibration. P_4 is the fourth Legendre polynomial evaluated in a similar manner; it may be evaluated by Raman scattering of the vibration bands corresponding to the C–C bonds.⁴¹ Their variation is not affected by chain length, it is slightly affected by melt temperature, and the stabilization of P_2 at 0.67 yields an average angle between adjacent chain segments in the LOR of $\approx 28^\circ$; the limiting angle in step 2 of the LOR's search was set at 40° . Squares (P_2) and circles (P_4) indicate the orientational correlations of Kuhn monomers for the bulk melt of C250 at 353 K (each monomer having 13 UA). The distinct values evaluated for $\langle P_2(\alpha) \rangle_r$ and Q_{11} result from their different evaluation procedure: the former was evaluated for each UA of

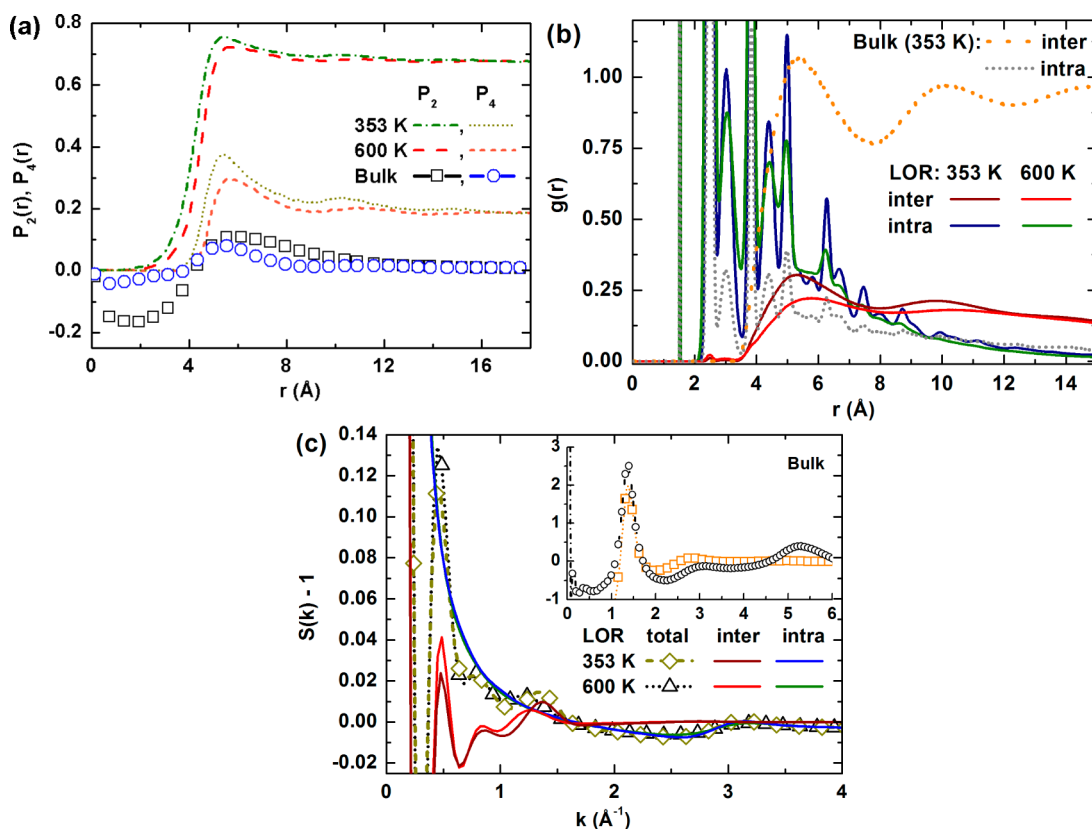


Figure 7. Structural characterization of the melt and of the short-range ordered regions for C250. (a) The second, P_2 , and fourth, P_4 , Legendre polynomial variation with the separation distance for segments connecting united atoms in the LOR (at 353 and 600 K) and for segments having one Kuhn monomer in length of bulk melt at 353 K (squares and circles). (b) Intermolecular and intramolecular radial distribution functions of the bulk melt (dashed and short-dotted lines) and of the ordered regions (solid lines). Note the enhancement of both inter and intramolecular correlations with the decrease of temperature. (c) Structure factor of the short-range ordered regions (LOR) showing peaks at $k = 0.45 \text{ Å}^{-1}$ and $k = 1.0 \text{ Å}^{-1}$ for both the intermolecular and total $S(k)$, and of the bulk melt (inset; C250 at 353 K). Squares and circles in the inset are for the intermolecular part and total of the system, respectively.

the ordered chain segment and the latter for the vector joining the first and last atoms of the ACS in the LOR. Differences in the orientational order are obvious among the local ordered regions and the bulk.

Further details on the short-range order are still provided for the same system by the radial distribution function (Figure 7b) and structure factor (Figure 7c)—see additional description of the evaluation procedure in Appendix IV. Short-range order in liquids is enhanced as its temperature is decreased. It is revealed by the increasing height and the narrowing width of the peaks in $g(r)$ and $S(k)$, mostly of those related to molecules located in the first coordination shell.⁴³ Sharper peaks are obtained at lower temperatures, both for the inter and intramolecular contributions, the first because van der Waals interaction energy between aligned chain segments increases with their length,^{47,48} Figure 6b, and the latter because low energy conformational states are more populated with the decreasing of temperature. Figure 7c displays the inter and intramolecular local structure factor at 353 and 600 K, while the inset shows the bulk structure factor. The LORs' intermolecular and total structure factor are different from those of the bulk (inset), presenting two peaks at k values of 0.46 \AA^{-1} and 0.75 \AA^{-1} , besides an additional peak at 1.27 \AA^{-1} . This last peak is assigned to correlations recorded in the first maxima of $g_{\text{inter}}(r)$ at $\sim 5.0 \text{ \AA}$, corresponding to the first coordination shell, and the other two peaks are linked to the second coordination shell, correlations between $\sim 8 \text{ \AA}$ and $\sim 13 \text{ \AA}$. Results of Figure 7, parts b and c, agree with those obtained by Mavrantzas et al. for a similar system.⁴⁹

3.4. Segments in Random Conformational Sequences between the Ordered Regions. Chain segments in random conformational sequences between the ordered regions, not included in the thinner tube defined above, have the molecular mass distribution depicted in Figure 8. This distribution is

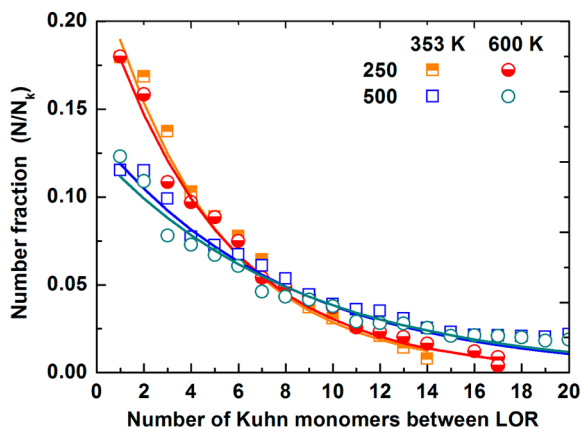


Figure 8. Molecular mass distribution for the chain segments in random conformational sequence (RCS) between the short-range ordered regions for C250 and C500 at the lowest and highest temperatures used in the simulations. Lines are fit to the data with Flory distribution; p values are in Table S2 of Supporting Information.

affected by temperature and chain length. It can be fitted to the Flory most-probable distribution, yielding a number-average molecular mass of $\sim 850 \text{ g/mol}$ and $\sim 1400 \text{ g/mol}$ for C250 and C500, respectively (see Table S1 of Supporting Information). Experimental values for the molecular mass between entanglements of this polymer are between 828 g/mol and 1850 g/mol .^{23,24}

3.5. Lifetime of Segments in Local Ordered Regions (LOR). Identification of ACS and of short-range order enables differentiating the different types of chains in the melt. Kuhn monomers in chains without any aligned chain segment, or having aligned chain segments not associated with any ordered region are classified as free chain segments (FC). Those segments in chains having at least one ordered region, which were identified as belonging to a LOR are classified as ordered segments (OS). Segments in random conformational sequences between the ordered regions are RCS, and those at the chain ends are CE. Because of the dynamic character of the ordered regions, segments identified at time zero as being part of a LOR may move later to a chain end (CE), to a RCS, or still to a free chain. The mobility of all these segments was evaluated, including those at the ordered regions. Details of this evaluation process and of the dynamics of the different chain segments are postponed to a future work.

To access the lifetime of segments at the ordered regions, all Kuhn segments participating in one ordered region at time zero, defined with the criterion described in section 3.2, were evaluated. Since generally the number of atoms classified as ACS belonging to a LOR is not a multiple of the number of segments existing in one Kuhn monomer, Kuhn monomers in the LORs were positioned at the center of the ACS.

These redefined segments in the LORs were relabeled as LOR (chain number, initial atom, final atom), where LOR stands for segments belonging to a local ordered region. Presence of these segments in a later time was identified for each frame, requiring that at least 70% of the atoms present at time zero in an ACS of a LOR still persist at time t (see sample of the code at the Supporting Information). Note that classification of segments as LOR implies always the interaction of an ACS with four other ACSs. Results of this evaluation for the system with 250 UA at 600 K are displayed in Figure 9a.

Figure 9b shows the orientational correlation of the Kuhn monomers of all chains at different times evaluated with the second order segmental orientation autocorrelation function, $C_2(t) = \langle 3[\mathbf{u}(t) \cdot \mathbf{u}(0)]^2 - 1 \rangle / 2$ where \mathbf{u} is a unit vector defining the CM position of the Kuhn monomers. Chain relaxation was also evaluated by following the time variation of the mean end-to-end distance of the chain normalized by its mean-square value at time zero, $\langle R(t) \cdot R(0) \rangle / \langle R^2(0) \rangle$. The orientational correlation decay of segments in the ordered regions is also presented.

As demonstrated in Figure 9a, atoms identified as belonging to an ACS, participating in short-range ordered regions, persist in time for times longer than the orientational relaxation time of the indistinguishable Kuhn monomers and still for times longer than the Rouse relaxation time of the chain, as measured by the decay to zero of $\langle R(t) \cdot R(0) \rangle / \langle R^2(0) \rangle$, at $\sim 31.6 \text{ ns}$. The decay to zero of $C_2(t)$ for segments at the ordered regions occurs at $\sim 3.1 \text{ ns}$. The dynamic character of segments at the ordered regions is also illustrated in Figure 9a: segments exist that belong to an ordered region at very short time, and migrate further to a chain end or to a random conformational sequence of chain segments.

4. DISCUSSION

All above evaluations were made with a single assumption, namely, that sequences of aligned chain segments with a length equal, at least, to the Kuhn monomer length may be defined by confining them to a tube section having a diameter lower than the diameter of one Kuhn monomer. The finding that chain

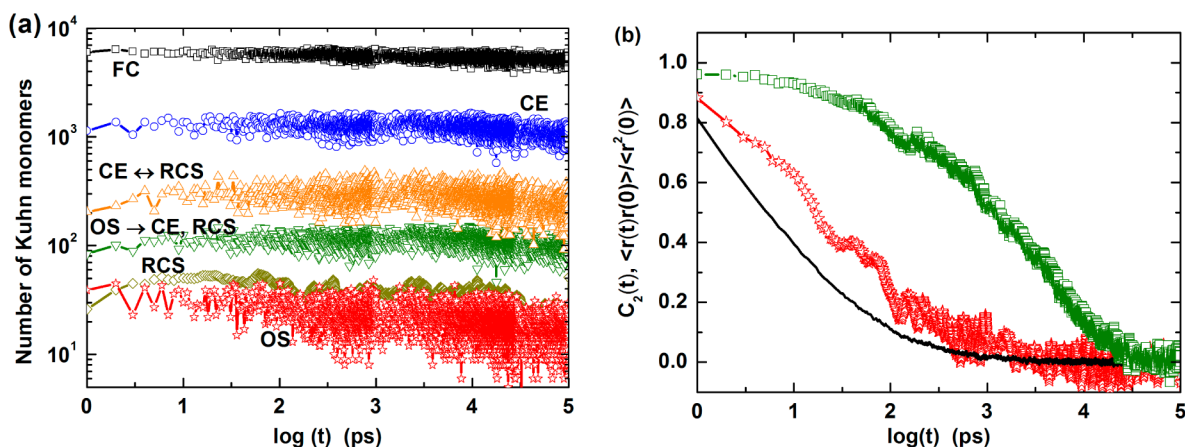


Figure 9. (a) Variation with time of the number of Kuhn monomers in different parts of the chain since time zero for C250 at 600 K: FC, free chains without any ordered segment; CE, segments at the chain ends, for chains with at least one ordered region; CE ↔ RCS, segments that moved from a chain end to a random conformational sequence between the ordered regions and vice versa; OS → RCS, CE, segments identified as part of an ordered region at time zero that moved latter to a RCS or to a CE; RCS, segments identified as RCS between the ordered regions; and OS, segments identified as belonging to ordered regions at time zero maintaining the same classification at later times. (b) Second order segmental orientation autocorrelation function for the indistinguishable Kuhn monomers of all chains (black line) and those at the ordered regions (red line and star). Squares in green indicate the orientational correlation of the end-to-end chain vector normalized by the mean end-to-end distance squared at time zero.

placement at the ordered regions resembles that existing in the solid phase, together with the persistence of these segments up to times longer than the Rouse relaxation time of the chain allow us to anticipate that short-range order, as identified in this work, should play an important role on the earlier crystallization stages, namely on the definition of precursor structures for crystallization. Future works on denser melts may provide this missing information.

Associated to density fluctuations in the melt resulting from the local ordered regions are also energy fluctuations. On the basis of results on previous works,^{44,47,48} the interaction energy between one Kuhn monomer of length 14 Å interacting with four other strictly parallel Kuhn monomers of the same length at 473 K is around 5.6 kJ mol⁻¹, while the melt thermal energy is around 3.9 kJ mol⁻¹. As shown in Figure 6b, Kuhn segments at the ordered regions may have higher length and the interaction energy of a segment at the center of an ordered region increases as $W \approx 4.01L$ kJ mol⁻¹, with the length of the aligned chain segments L in Angstrom; the number 4 stands for the number of ACS interacting with a segment at the center as in Figure 5b. Therefore, the interaction energy of segments in the LOR may surpass the 5.6 kJ mol⁻¹ indicated above, although a more precise evaluation requires further data analysis. It should consider, besides the distance and length of the interacting chain segments, the angle between them. On the basis of this estimate, we may foresee that the segments in the ordered regions should play an important role on chain dynamics at the molten state, relaxing slower than other, nonaligned chain segments. This slower relaxation is demonstrated in Figure 9b, where the orientational relaxation of Kuhn monomers at the ordered regions may be compared with that of the indistinguishable Kuhn monomers (monomers not classified with respect to their position in the chain). Since one Kuhn monomer contains around 13 UA, it is expected that its orientational relaxation should be retarded when compared to the torsional time autocorrelation function of segments within those Kuhn monomers as evaluated for example by Harmandaris et al.⁵⁰

Because shear flow has an elongational component, besides a rotational component, it is expected that local ordered regions are enhanced upon the application of shear, explaining therefore the origin of shear-induced precursor structures and also shedding light onto the origin of melt memory effect. The persistence of ordered regions for times longer than the longest relaxation time of the chain, as demonstrated in Figure 9a, justifies this assumption. It must be stressed that the conjectures made in this Discussion on the relationship between short-range order, the precursor structures for crystallization, and the origin of melt memory effect still require validation. However, short-range range order seems to be a good starting point for ascertaining their validity.

It is known that dynamical processes are always controlled by the slowest mechanism. Our results have shown that orientational relaxation of Kuhn monomers at the ordered regions is slower than that of monomers in other parts of the chain. It remains to be seen up to what extend ordered regions having a volume of $\approx 17^3$ Å³, evaluated from results in Figures 6b and 7b, occupying a volume fraction as low as $\sim 4\%$, play any relevant role in those processes. Also to be explored in future works is the effect of flow and lowering of temperature in the size and volume fraction of these ordered regions.

5. CONCLUSIONS

We demonstrated the existence of short-range order in unentangled and entangled polyethylene melts. The demonstration was made by defining sequences of aligned chain segments having at least the length of one Kuhn monomer. Interactions of one aligned chain segment with other neighboring aligned chain segments allowed the definition of short-range order, i.e. local ordered regions. The length of segments in these regions increases by decreasing temperature and increasing the chain length. Ordered regions acquire the shape of prolate ellipsoid at lower temperature. Chain placement in these regions resembles that existing in the crystalline unit cell at the solid state, and they persist for a time longer than the Rouse relaxation time of the chain. The local structure factor of segments in these regions indicate

correlations between chain segments at k values below 1 \AA^{-1} , which are completely absent when similar analysis is made unselectively over the whole melt. The chain length variation of the local order parameter, evaluated by the first eigenvalue of the ordering tensor, agrees with experimental results, although these last results were obtained for a different system. Overall, these results allow us to conclude that short-range order in polyethylene melts resembles a dynamic uniaxial nematic phase. Furthermore, it was shown that the molecular mass distribution of segments in random conformational sequences between the ordered regions follows the Flory distribution, and the number-average molecular mass compares with the experimental values for the molecular mass between entanglements.

■ APPENDIX I: LOCAL RADIUS OF GYRATION TENSOR

The radius of gyration tensor⁵¹ was evaluated at each temperature for all chains in the ensemble and locally, for all identified ordered regions. For an ensemble of n_{ch} chains, each having n_{at} atoms, the gyration tensor is

$$\langle \bar{R}_g \rangle = \frac{1}{n_{ch}} \frac{1}{N_{at}} \sum_{j=1}^{n_{ch}} \sum_{i=1}^{n_{at}} (\vec{r}_{ji} - \vec{r}_{CM,j})^2 \quad (3)$$

where the index i runs over all atoms in each chain, the index j runs over all chains in the box, and $\vec{r}_{CM,j}$ are the center of mass coordinates of the j chain.

The radius of gyration tensor for each ordered region was evaluated as

$$\bar{R}_{g,LOR} = \frac{1}{n_{ch,LOR}} \frac{1}{n_{at,ACS}} \sum_{j=1}^{n_{ch,LOR}} \sum_{i=1}^{n_{at,ACS}} (\vec{r}_{ji} - \vec{r}_{CM,j})^2 \quad (4)$$

where $n_{ch,LOR}$ is the number aligned chain segments (ACS) in one local ordered region (minimum five, according to the search criteria defined), which may belong to the same chain or to different chains, and $n_{at,ACS}$ are the number of united atoms in each aligned chain segment, not necessarily the same for all segments within an ordered region. Data in Table 3 was obtained after taking the ensemble average over all local ordered regions (n_{LOR}) identified in one time frame and over 1000 frames separated by 0.1 ns during the 100 ns of equilibration time

$$\langle \bar{R}_{g,LOR} \rangle = \frac{1}{n_{LOR}} \frac{1}{n_{ch,LOR}} \frac{1}{n_{at,LOR}} \sum_{k=1}^{n_{LOR}} \sum_{j=1}^{n_{ch,LOR}} \sum_{i=1}^{n_{at,LOR}} (\vec{r}_{kji} - \vec{r}_{CM,k,j})^2 \quad (5)$$

$\vec{r}_{CM,k,j}$ is the center of mass coordinates of the aligned chain segment j in the local ordered region k .

■ APPENDIX II: LOCAL ORDER TENSOR

The evaluation of the order tensor was made, as in ref 52, by defining a vector \vec{v}_{i-f} joining the initial and final atoms in each aligned chain segment of an ordered region. The x , y , z components of the \vec{v}_{i-f} unit vector are $\hat{u}_{\alpha(\beta)} = \vec{v}_{i-f,\alpha(\beta)} / |\vec{v}_{i-f,\alpha(\beta)}|$, with α (or β) = (x , y , z). The order tensor of a single ordered region is defined by the real symmetric matrix^{41,52}

$$\bar{Q}_{\alpha\beta} = \frac{1}{n_{ch,LOR}} \sum_{j=1}^{n_{ch,LOR}} \left(\frac{3}{2} \hat{u}_{j\alpha} \cdot \hat{u}_{j\beta} - \frac{1}{2} \delta_{\alpha\beta} \right) \quad (6)$$

where the summation, as in eq 4 is made over all aligned chain segments belonging to a LOR, and $\delta_{\alpha\beta}$ is the Kronecker delta. The ensemble and time average was taken similarly as in the local radius of gyration tensor evaluation:

$$\langle \bar{Q}_{\alpha\beta} \rangle = \frac{1}{n_{LOR}} \frac{1}{n_{ch,LOR}} \sum_{k=1}^{n_{LOR}} \sum_{j=1}^{n_{ch,LOR}} \left(\frac{3}{2} \hat{u}_{j\alpha} \cdot \hat{u}_{j\beta} - \frac{1}{2} \delta_{\alpha\beta} \right) \quad (7)$$

■ APPENDIX III: ORIENTATIONAL CORRELATIONS

Local orientation of polymer chain segments in the bulk melt and at the ordered regions was evaluated with the orientational correlation function. The second-order Legendre polynomial

$$\langle P_2(\alpha) \rangle_r = \frac{1}{2} \langle 3\cos^2(\alpha) - 1 \rangle_r \quad (8)$$

was used to access orientation between neighboring chain segments. The scalar product between the unit vector of segment i of chain k and segment j of chain l describes the angle between chain tangent vectors,

$$\cos(\alpha) = \hat{u}_{l,j} \cdot \hat{u}_{k,i} = \frac{\vec{r}_{l,j} - \vec{r}_{l,j-1}}{|\vec{r}_{l,j} - \vec{r}_{l,j-1}|} \cdot \frac{\vec{r}_{k,i} - \vec{r}_{k,i-1}}{|\vec{r}_{k,i} - \vec{r}_{k,i-1}|} \quad (9)$$

The orientational correlation of the bulk melt displayed in Figure 7a was evaluated in Kuhn monomer steps, $\hat{u}_i = \vec{r}_i - \vec{r}_{i-nKuhn} / |\vec{r}_i - \vec{r}_{i-nKuhn}|$. That of segments in the ordered regions was evaluated segment by segment, a segment connecting two consecutive united atoms.

The fourth-order Legendre polynomial was evaluated as

$$\langle P_4(\alpha) \rangle_r = \frac{1}{8} \langle 35\cos^4(\alpha) - 30\cos^2(\alpha) + 3 \rangle_r \quad (10)$$

■ APPENDIX IV: PAIR DISTRIBUTION FUNCTION AND STRUCTURE FACTOR

Information about the structure of the melt was obtained by evaluating the pair (or radial) distribution function and the structure factor resulting from intramolecular and intermolecular interactions. The intramolecular pair distribution function at a specific distance r was evaluated as

$$g_{int\ ra}(r) = \frac{\rho_N}{n_{ch} n_{at}} \sum_{k=1}^{n_{ch}} \left(\sum_{j=1}^{n_{at}} \sum_{i=1}^{n_{at}} \delta(r - r_{k,ij}) \right)_{i \neq j} \quad (11)$$

where ρ_N is the number density of atoms in the ensemble, n_{at} the number of atoms per chain, n_{ch} the number of chains existing in the ensemble, $r_{k,ij}$ is the distance between atoms i and j of chain k , and δ is the Dirac delta function.

The intermolecular pair distribution function accounts for interactions between atoms of different chains. It was evaluated as

$$g_{int\ er}(r) = \frac{\rho_N}{n_{ch} \cdot n_{at}} \sum_{l=1}^{n_{ch}} \sum_{k=1}^{n_{ch}} \left(\sum_{j=1}^{n_{at}} \sum_{i=1}^{n_{at}} \delta(r - r_{lk,ji}) \right)_{k \neq l} \quad (12)$$

where $r_{lk,ji}$ is the distance separating atom i from atom j of the chains k and l , respectively.

Both in eqs 11 and 12, a cutoff distance r was set at half the box length. The total pair distribution function is obtained by adding these two contributions. In the evaluations made for the local pair distribution function, the application of eqs 11 and 12

was restricted to the aligned chain segments in the local ordered regions,

$$g_{int\ ra,Local}(r) = \frac{\rho_N}{n_{ch,LOR}n_{at,ACS}} \sum_{k=1}^{n_{ch,LOR}} \left(\sum_{j=1}^{n_{at,ACS}} \sum_{\substack{i=1 \\ i \neq j}}^{n_{at,ACS}} \delta(r - r_{k,ji}) \right) \quad (13)$$

and

$$g_{int\ er,Local}(r) = \frac{\rho_N}{n_{ch,LOR}n_{at,ACS}} \sum_{l=1}^{n_{ch,LOR}} \sum_{k=1}^{n_{ch,LOR}} \left(\sum_{j=1}^{n_{at,ACS}} \sum_{i=1}^{n_{at,ACS}} \delta(r - r_{lk,ji}) \right) \quad (14)$$

The product $n_{ch,LOR}n_{at,ACS}$ gives the number of atoms in one ordered region. Results displayed in Figure 7b are an ensemble average for all ordered regions present in one time frame and a time average of 1000 frames separated from each other by 0.1 ns. In eqs 13 and 14 ρ_N could have been replaced by the ratio between the volume of an ordered region and the number of atoms selected as being part of that ordered region. The effect would be a vertical shift in the ordinates of the curves for $g_{inter,Local}$ and $g_{inter,Localb}$ without affecting further the results obtained.

The pair distribution function is correlated to the static structure factor through a 1-D Fourier transform. Under the assumption of melt isotropy, the result is

$$S(k) = 1 + \frac{4\pi\rho_N}{k} \int_0^\infty [g(r) - 1] r \sin(kr) dr \quad (15)$$

Evaluations of the intramolecular and intramolecular contributions for the structure factor followed the procedure described in ref 53.

■ ASSOCIATED CONTENT

■ Supporting Information

Packing length values and the diameter of the Kuhn monomer evaluated for two representative temperatures (Table S1), values for the number-average molecular mass distribution of segments in random conformational sequences between the ordered regions evaluated by counting the number of atoms, as well as p values of the Flory distribution (Table S2), values for chain length variation of the local order parameter tensor first eigenvalue with experimental results obtained by NMR on 1,4-polybutadiene (Figure S1), and two samples of the code used, one for the identification and labeling of aligned chain segments in Figure 4 and the other for evaluating the lifetime time and orientational correlation of segments at the ordered regions. This material is available free of charge via the Internet at <http://pubs.acs.org>.

■ AUTHOR INFORMATION

Corresponding Author

*E-mail: (J.A.M.) jamartins@dep.uminho.pt.

Author Contributions

N.M.M. performed the molecular mechanics simulations, and contributed to the manuscript writing. J.A.M. idealized the simulation experiments, conceived the data analysis code, made the data interpretation, and wrote the manuscript.

Notes

The authors declare no competing financial interest.

■ ACKNOWLEDGMENTS

We acknowledge Vitor Felix for making available computer facilities at the University of Aveiro that were used at the start of this work. We thank discussions with Ralph Colby and Loic Hilliou. This work was in part financially supported by FCT through PEst-C/QUI/UI0686/2011, FCOMP-01-0124-FEDER-022716 and PEst-C/CTM/LA0011/2011 programs. The authors thank the access to the Minho University GRIUM cluster and for contract research grant C2008-UMINHO-CQ-03.

■ ABBREVIATIONS

ACS, aligned chain segments; LOR, local ordered regions

■ REFERENCES

- (1) Flory, P. J. *Faraday Discuss. Chem. Soc.* **1979**, 68, 14–25.
- (2) de Gennes, P. G. *Scaling Concepts in Polymer Physics*; Cornell University Press: Ithaca, NY, 1979.
- (3) Doi, M.; Edwards, S. F. *The Theory of Polymer Dynamics*; Oxford Univ. Press Inc.: New York, 1986.
- (4) McLeish, T. C. B. *Adv. Phys.* **2002**, 51, 1379–1527.
- (5) Wittmer, J. P.; Beckrich, P.; Johnner, A.; Semenov, A. N.; Obukhov, S. P.; Meyer, H.; Baschnagel, J. *Europhys. Lett.* **2007**, 77, 56003.
- (6) Wittmer, J. P.; Beckrich, P.; Meyer, H.; Cavallo, A.; Johnner, A.; Baschnagel, J. *Phys. Rev. E* **2007**, 76, 11803.
- (7) Collin, D.; Martinoty, P. *Physica A* **2003**, 320, 235–248.
- (8) Mendil, H.; Baroni, P.; Noirez, L. *Eur. Phys. J. E* **2006**, 19, 77–85.
- (9) McKenna, G. B. *Eur. Phys. J. E* **2006**, 19, 101–108.
- (10) Vlassopoulos, D. *Eur. Phys. J. E* **2006**, 19, 113–117.
- (11) Zondervan, R.; Kulzer, F.; Berkhout, G. C. G.; Orriit, M. *Proc. Natl. Acad. Sci. U.S.A.* **2007**, 104, 12628–12633.
- (12) Fisher, E. W.; Strobl, G. R.; Dettenmaier, M.; Stamm, M.; Steidle, N. *Faraday Discuss. Chem. Soc.* **1979**, 68, 26–45.
- (13) Graf, R.; Heur, A.; Spiess, H. W. *Phys. Rev. Lett.* **1998**, 80, 5738–5741.
- (14) Tracht, U.; Wilhelm, M.; Heuer, A.; Feng, H.; Schmidt-Rohr, K.; Spiess, H. W. *Phys. Rev. Lett.* **1998**, 81, 2727–2730.
- (15) Londono, J. D.; Habenschuss, A.; Curro, J. G.; Rajasekaran, J. J. *J. Polym. Sci. Part B. Polym. Phys.* **1996**, 34, 3055–3061.
- (16) Mitchell, G. R.; Rosi-Schwartz, B.; Ward, D. J. *Philos. Trans. R. Soc. London, A* **1994**, 348, 97–115.
- (17) Rigby, D.; Roe, R.-J. *J. Chem. Phys.* **1988**, 89, 5280–5290.
- (18) Paul, W.; Yoon, D. Y.; Smith, G. D. *J. Chem. Phys.* **1995**, 103, 1702–1709.
- (19) Weber, W.; Paul, W.; Kob, W.; Binder, K. *Phys. Rev. Lett.* **1997**, 78, 2136–2139.
- (20) Abrams, C. F.; Kremer, K. *J. Chem. Phys.* **2001**, 115, 2776–2785.
- (21) Paul, W.; Smith, G. D.; Yoon, D. Y. *Macromolecules* **1997**, 30, 7772–7780.
- (22) Gee, R. H.; Lacevic, N.; Fried, L. E. *Nat. Mater.* **2006**, 5, 39–43.
- (23) Liu, C.; He, J.; van Ruymbeke, E.; Keunings, R.; Bailly, C. *Polymer* **2006**, 47, 4461–4479.
- (24) Dealy, J. M.; Larson, R. G. *Structure and rheology of molten polymers: from structure to flow behaviour and back again*; Carl Hanser Verlag: Munich, Germany, 2006.
- (25) Martínez, L.; Andrade, R.; Birgin, E. G.; Martínez, J. M. *J. Comput. Chem.* **2009**, 30, 2157–2164.
- (26) Brown, D.; Clarke, J. H. R.; Okuda, M.; Yamakazi, T. *J. Chem. Phys.* **1994**, 100, 1684–1692.
- (27) Brown, D.; Clarke, J. H. R.; Okuda, M.; Yamakazi, T. *J. Chem. Phys.* **1994**, 100, 6011–6018.

- (28) Paul, W.; Binder, K.; Heermann, D. W.; Kremer, K. *J. Chem. Phys.* **1991**, *95*, 7726–7740.
- (29) Hess, B.; Bekker, H.; Berendsen, H. J. C.; Fraaije, J. G. E. M. *J. Comput. Chem.* **1997**, *18*, 1463–1472.
- (30) Hess, B.; Kutzner, C.; van der Spoel, D.; Lindahl, E. *J. Chem. Theory Comput.* **2008**, *4*, 435–447.
- (31) Evans, D. J.; Holian, B. L. *J. Chem. Phys.* **1985**, *83*, 4069–4074.
- (32) Parrinello, M.; Rahman, A. *J. Appl. Phys.* **1981**, *52*, 7182–7190.
- (33) Orwoll, R. A. In *Physical properties of polymers*; 2nd ed., Mark, J. E., Ed.; Springer: Berlin, 2007; Chapter 7.
- (34) Foteinopoulou, K.; Karayiannis, N. C.; Laso, M.; Kröger, M. *J. Phys. Chem. B* **2009**, *113*, 442–455.
- (35) Ding, A.; Kisluk, A.; Sokolov, A. P. *Macromolecules* **2004**, *37*, 161–166.
- (36) Rubinstein, M.; Colby, R. *Polymer Physics*; Oxford Univ. Press Inc.: New York, 2003.
- (37) Alexiadis, O.; Mavrantzas, V. G.; Khare, R.; Beckers, J.; Baljon, A. R. C. *Macromolecules* **2008**, *41*, 987–996.
- (38) Fetters, L. J.; Lohse, D. J.; Richter, D.; Witten, T. A.; Zirkel, A. *Macromolecules* **1994**, *27*, 4639–4647.
- (39) Ramos, J.; Peristeras, L. D.; Theodorou, D. N. *Macromolecules* **2007**, *40*, 9640–9650.
- (40) Hoshen, J.; Kopelman, R. *Phys. Rev. B* **1976**, *14*, 3438–3445.
- (41) de Gennes, P. G.; Prost, J. *The Physics of Liquid Crystals*; Oxford Univ. Press Inc.: New York, 1993.
- (42) Sherrell, P. L.; Crellin, D. A. *J. Phys. (Paris)* **1979**, *40*, 211–216.
- (43) March, N. M.; Tosi, M. P. *Introduction to Liquid State Physics*; World Scientific Publishing Co. Pte. Ltd.: Singapore, 2002.
- (44) Martins, J. A. *J. Macromol. Sci., Part B* **2011**, *50*, 769–794.
- (45) Kariyo, S.; Brodin, A.; Gainaru, C.; Herrmann, J.; Shick, H.; Novikov, V. N.; Rössler, E. A. *Macromolecules* **2008**, *41*, 5313–5321.
- (46) Kariyo, S.; Brodin, A.; Gainaru, C.; Herrmann, J.; Hintermeyer, H.; Shick, H.; Novikov, V. N.; Rössler, E. A. *Macromolecules* **2008**, *41*, 5322–5332.
- (47) Salem, L. *J. Chem. Phys.* **1962**, *37*, 2100–2113.
- (48) Martins, J. A. *Macromol. Theory Simul.* **2010**, *19*, 360–369.
- (49) Mavrantzas, V. G.; Boone, T. D.; Zervopoulou, E.; Theodorou, D. N. *Macromolecules* **1999**, *32*, 5072–5096.
- (50) Harmandaris, V. A.; Mavrantzas, V. G.; Theodorou, D. N. *Macromolecules* **1998**, *31*, 7934–7943.
- (51) Theodorou, D. N.; Sutter, U. W. *Macromolecules* **1985**, *18*, 1206–1214.
- (52) Hudzinsky, D.; Lyulin, A. v.; Baljon, A. R. C.; Balabaev, N. K.; Michels, M. A. J. *Macromolecules* **2011**, *44*, 2299–2310.
- (53) Paul, W.; Smith, G. D. *Rep. Prog. Phys.* **2004**, *67*, 1117–1185.

Supporting Information

for

Short-Range Order in Polyethylene Melts: Identification and Characterization

José A. Martins,^{†,‡,*} and Nuno M. Micaelo[§]

[†] Departamento de Engenharia de Polímeros, Universidade do Minho, Campus de Azurém 4800-058 Guimarães, Portugal.

[‡] CICECO, Universidade de Aveiro, 3810-193 Aveiro, Portugal

[§] Departamento de Química, Centro de Química, Universidade do Minho, Campus de Gualtar 4710-057 Braga, Portugal.

Correspondence to: jamartins@dep.uminho.pt

Contents:

Tables S1

Figure S1

Samples of code

Supporting Information

SI Tables

Table S1. Number average molecular mass evaluated by fitting the data in Fig. 1C with the most probable distribution $(1-p)p^{x-1}$; p values are indicated. Also indicated are the values directly obtained from the program by counting the number of segments in random conformational sequences between the ordered regions. For all estimations made with the program the standard deviation of the mean is less than 8% of the mean result shown in the table.

<i>N = 250; M = 3500 g/mol</i>				<i>N = 500; M = 7000 g/mol</i>		
T (K)	<i>Mn – Flory</i> (g/mol)	<i>p</i>	<i>Mn</i> <i>program</i> (g/mol)	<i>Mn – Flory</i> (g/mol)	<i>p</i>	<i>Mn</i> <i>program</i> (g/mol)
353	978.6	0.811	850.3	1556.8	0.881	1442.2
373	--	--	837.5	--	--	1321.6
393	--	--	847.0	--	--	1353.2
415	--	--	886.1	--	--	1276.9
500	--	--	725.6	--	--	1402.3
600	883.6	0.821	806.4	1413.5	0.888	1426.7

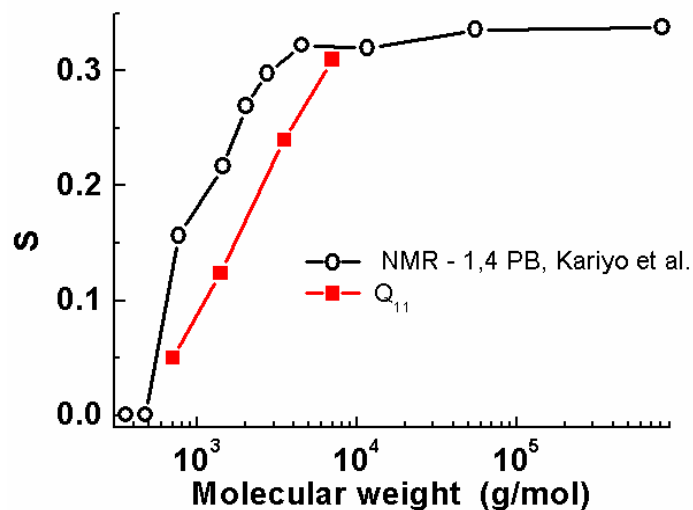


Figure S1. Molecular weight variation of local order parameter S (or Q_{11}). Comparison of experimental results obtained from fast field cycling NMR studies on the dispersion of the ^1H spin-lattice relaxation time of linear 1,4-polybutadienes (7) with the first eigenvalue of the local order tensor for the systems with 50 UA, 100 UA, 250 UA and 500 UA evaluated at 353 K (temperature value similar to that of experimental results in ref. 7).

Sample of Fortran code for identifying the sequences of ordered chain segments

In this code section, reference vector is the vector joining the first and last atoms of one Kuhn monomer. It is defined in the loop AtL_i1. The loop increment was selected as half the number of segments in one Kuhn monomer. All atoms afterwards are the running vector. They are tested and eventually selected as being part of an ordered sequence of chain segments. This procedure allows defining ordered sequences of chain segments anywhere in the chain, including at the very first atoms near the chain ends. The validity of this criterion may be confirmed by a visual inspection of the defined ordered sequences, as shown in Fig. 1. In sample of code below CosAng and NormVector are functions defined in the code.

Sample of the code in fortran:

```
! Part I.
! Defines the number of segments (united atoms) laying inside of a thinner tube
! define the loop step
LoopStep = Anint(Float(NSeg/2))
! cycle over all chains in the box
ChL_i1: Do iCh = 1, ChN
!cycle over all atoms in the chain
  AtL_i1: Do iAt = 1, nChAt, LoopStep
    !evaluate the distance between the initial atom and the final atom of the loop step;
    ! same for y and z coordinates
    xVr = xi ( iCh, iAt + NSeg ) - xi ( iCh, iAt)
    ! correct for the periodic boundary conditions
    xVr = xVr - BoxX* Anint (xVr/BoxX)
    ! Test the position of each atom in the loop step from iAt to iAt + NSeg - 1
    SegL: Do jAt = iAt + 1, iAt + NSeg - 1
      xRunDiff = xi ( iCh, jAt ) - xi ( iCh, iAt )
      ! correct for the periodic boundary conditions
      xRunDiff = xRunDiff - BoxX* Anint (xRunDiff/BoxX)
      !Evaluate the angle between the lines joining
        ! Line 1. the initial atom and the running atom within the loop step, and
        ! Line 2. the initial atom and the final atom of the loop step
      Alfa = Acos(CosAng( xRunDiff, yRunDiff, zRunDiff, xVr, yVr, zVr ) )
      ! Evaluate the distance between the running atom and Line 2

      DistRunVect_RefVect = Sin (Alfa)* NormVector (xRunDiff, yRunDiff , zRunDiff )
      ! Accept or reject the atom as part of a chain segment located inside of a thinner tube
      If (DistRunVect_RefVect <= CriticalDist ) Then
        ! accept and label; the assignment could be the evaluated distance or the number 1
        TubeR (iCh, jAt ) = DistRunVect_RefVect
      End If
    End Do SegL
  End Do AtL_i1
End Do ChL_i1
```



```

End Do AtL_i1
End Do ChL_i1

```

! Part II.

! Counts the number of selected segments and accepts sequences when the number of selected segments is equal or greater than those existing one Kuhn monomer.

Counter = 0

```

ChL_i2: Do iCh = 1, ChN

```

```

    AtL_i2: Do iAt = 2, nChAt

```

```

        If ( (TubeR (iCh, iAt == 0.0) .AND. (TubeR (iCh, iAt - 1) > 0.0) ) Then

```

```

            Counter = 0

```

```

            Cycle AtL_i2

```

```

        Else If (TubeR (iCh, iAt) == 0.0) Then

```

```

            Cycle AtL_i2

```

```

        Else If (TubeR (iCh, iAt) > 0.0) Then

```

```

            Counter = Counter + 1

```

```

            If (TubeR (iCh, iAt + 1) > 0.0) Cycle AtL_i2

```

```

        End If

```

```

        ! execute the next steps only when TubeRadius (iCh, iAt) > 0.0 and

```

```

        ! TubeRadius (iCh, iAt + 1) = 0.0

```

```

        If (Counter >= NSegs ) Then

```

```

            SegL_2: Do jAt = iAt - Counter, iAt

```

```

                TubeRFinal (iCh, jAt) = TubeR (iCh, jAt)

```

```

            End Do SegmLoop2

```

```

        ! Reset the counter

```

```

        Counter = 0

```

```

        End If

```

```

    End Do AtL_i2

```

```

End Do ChL_i2

```

Sample of the code used in the evaluations made in Figs. 9a and 9b.

Ordered chain segments participating in local ordered regions having at least the length of one Kuhn monomer, or multiples of it, are labelled as True for all frames, frame zero, and all others. The following analysis used this definition used the arrays OSz for frame zero and OZt for any other subsequent frame.

...

....

Check = .True.

```

Ch_OS_L1: Do iCh = 1, ChN

```

```

    !cycle over all chains in the BOX at time ZERO

```

```

    CountAt = 0

```

```

    At_OS_L1: Do iAt = 1, nChAt

```

```

        ! cycle over all atoms in the chain – time ZERO

```

```

        If (iAt + NSeg > nChAt) Cycle Ch_OS_L1

```

```

! *****
! TEST ALL CHAIN SEGMENTS ASSOCIATED TO LOCAL ORDERED REGIONS
! IN FRAME ZERO
OS_z: If (OSz(iCh,iAt)) Then
! An OS of FRAME zero was identified with initial atom = iAt
    CountAt = CountAt + 1

! &&&&&& CHECK at time t
! THEN CHECK IF A CORRESPONDING ORDERED SEQUENCE EXISTS AT TIME t
    If (Check) Then
        Check_OS: Do i = iAt, iAt+NSeg-1
! OSt is TRUE if atom i in chain iCh was identified as belonging to a LOR
            If (OSt(iCh, i)) Then
                Count_t = Count_t + 1
            End If
        End DO Check_OS
    End If
! &&&&&&
! NO ORDERED SEGMENT EXISTS AT TIME t ... cycle
If (CountAt == 1 .AND. Count_t == 0) Then
    CountAt = 0
    Cycle At_OS_L1
!
! The OS was detected in two frames - Evaluate the MSD and other quantities
! THIS IS THE CRITERIA USED TO ENSURE THAT AT LEAST 70% OF ORDERED
! SEGMENTS AT TIME - t - ARE EXACTLY THE SAME AS THOSE EXISTING IN
! THE REFERENCED SEGMENT AT TIME ZERO.
    Else If (Count_t >= Int(0.7*NSeg) .AND. CountAt == 1) Then
        j = iAt
        ! Start now the evaluations...
...
        ! For P2OS
        xz = xi_cz(iCh, j+NSeg-1) - xi_cz(iCh, j)
        yz = yi_cz(iCh, j+NSeg-1) - yi_cz(iCh, j)
        zz = zi_cz(iCh, j+NSeg-1) - zi_cz(iCh, j)
        xt = xi_ct(iCh, j+NSeg-1) - xi_ct(iCh, j)
        yt = yi_ct(iCh, j+NSeg-1) - yi_ct(iCh, j)
        zt = zi_ct(iCh, j+NSeg-1) - zi_ct(iCh, j)

        xz = xz - BoxXz* Anint(xz/BoxXz)
        yz = yz - BoxXz* Anint(yz/BoxXz)
        zz = zz - BoxXz* Anint(zz/BoxXz)
        xt = xt - BoxXt* Anint(xt/BoxXt)
        yt = yt - BoxXt* Anint(yt/BoxXt)
        zt = zt - BoxXt* Anint(zt/BoxXt)

```

```

! .... Evaluate C2(t)
P2Dummy = (CosAng(xt, yt, zt, xz, yz, zz))*2 + P2Dummy
! Count the number of ordered segment. Reset after comparing two frames, zero and t
Count_OS = Count_OS + 1
Check = .False.

! is inside and OS already detected. Cycle
Else If (Count_t > 0 .AND. CountAt < NSeg ) Then
  !write (*,*) 'CountAt', CountAt
  Cycle At_OS_L1
!
! Has reached the limiting number of segments within an OS
Else If (Count_t > 0 .AND. CountAt == NSeg ) Then
  CountAt = 0
  Count_t = 0
  Check = .True.
  Cycle At_OS_L1
End If
End If OS_z
! *****

End Do At_OS_L1
End Do Ch_OS_L1

P2OS = 0.5*(3.0*P2Dummy/Float(Count_OS) - 1.0)

```